On the nature of $a_1(1420)$

M. Mikhasenko,[1] B. Ketzer,[1] and A. Sarantsev[1,2]

[1] *Universität Bonn, Helmholtz-Institut für Strahlen- und Kernphysik, 53115 Bonn, Germany*

[2] *Petersburg Nuclear Physics Institute, Gatchina, Russia*

The resonance-like signal with axial-vector quantum numbers $J^{PC} = 1^{++}$ at a mass of 1420 MeV and a width of 140 MeV, recently observed by the COMPASS and VES experiments in the $f_0(980)\pi$ final state and tentatively called $a_1(1420)$, is discussed. Instead of a genuine new meson, we interpret this signal as a dynamical effect due to a singularity (branching point) in the triangle diagram formed by the processes $a_1(1260) \to K^\star\bar{K}$, $K^\star \to K\pi$, and $K\bar{K} \to f_0(980)$ (+ c.c). The amplitude for this diagram is calculated. The result exhibits a peak in the intensity with a sharp phase motion with respect to the dominant $a_1(1260) \to \rho\pi$ S-wave decay, in good agreement with the data. The branching ratio of $a_1(1260) \to f_0(980)\pi$ via the triangle diagram is estimated and compared to the dominant decay $a_1(1260) \to \rho\pi$.

I. INTRODUCTION

Understanding the quark interaction at low and intermediate energies is one of the most challenging tasks of the theory of the strong interactions. To create a theoretical non-perturbative approach or, at least, to build a reliable model one should understand the nature of strongly interacting particles and their excitation spectrum. The classical quark model assumes that mesons are bound states of quarks and antiquarks, and groups the low-mass states into nonets with the same spin J, parity P and charge-conjugation parity C, with fixed mass differences between nonet members. The second assumption is that the quark-antiquark interaction at large distances is governed by a linearly rising potential which explains the phenomenon of quark confinement and predicts the full spectrum of quark-antiquark excited states. The success of the quark model is indisputable: most of the known mesons correspond very well to the predicted scheme [1].

However, it seems that the meson spectrum is notably richer than that predicted by the quark model. There is a growing set of experimental observations of resonance-like structures in partial waves with quantum numbers which are forbidden for the quark-antiquark system or situated at masses which can not be explained by the quark-antiquark model, see e.g. [2, 3] and references therein.

Recently the COMPASS [4–6] experiment reported the observation of a small resonance-like signal with axial-vector quantum numbers $I^G(J^{PC}) = 1^-(1^{++})$ in the $f_0(980)\pi$ P-wave of the $\pi^-\pi^-\pi^+$ final state, produced by diffractive scattering of a 190 GeV π^- beam on a proton target. The signal was also confirmed by the VES experiment [7] in the $\pi^-\pi^0\pi^0$ final state. In both experiments, the three-pion final states were analyzed using a two-step partial-wave analysis (PWA) technique. In the first step the data were grouped in small bins of 3π-invariant mass and momentum transfer. The isobar model was employed to parametrize possible decays to three final pions. An isolated, relatively narrow peak was found in the intensity of the 1^-1^{++} $f_0\pi$ P-wave at a mass around 1.4 GeV, accompanied by a sharp phase motion of this wave relative to other known resonances, with a phase variation exceeding 180°. In the second step of the COMPASS and VES analyses the spin-density matrix resulting from the first step was fitted with a model including Breit-Wigner resonances and background contributions. The new signal was described rather well with a hitherto unknown resonance, which was tentatively called $a_1(1420)$ with a mass $M_{a_1} \approx 1.42$ GeV and

width $\Gamma_{a_1} \approx 0.14\,\mathrm{GeV}$. The interpretation of this signal as a new state in the framework of the quark model is difficult. It cannot be a radial excitation of $a_1(1260)$ which is expected to have a mass above 1650 MeV. It is also not expected that the radial excitation has a width which is much smaller than the one of the ground state. Therefore, this signal is to be considered either as a strong candidate for a four-quark bound state or a meson-meson molecular bound state or to be explained as a some dynamical effect resulting from multi-particle interaction.

In the present paper we show that a signal of comparable strength, including the rapid phase motion, can be expected by the opening of the $K^\star\bar{K}$ decay channel for the isovector $a_1(1260)$, and the re-scattering of the kaons. There are two isospin combinations of intermediate particles:

(i) $a_1^-(1260) \to K^{\star 0}K^- \to \pi^- K^+ K^- \to \pi^- f_0$,

(ii) $a_1^-(1260) \to K^{\star -}K^0 \to \pi^- \bar{K}^0 K^0 \to \pi^- f_0$.

The corresponding triangle diagram has a logarithmic singularity on the tail of the wide $a_1(1260)$ which is due to a very peculiar kinematic situation, in which all intermediate particles are almost on their mass shell, causing a resonance-like effect.

Recently, Wu et al. [8, 9] showed that the same triangle singularity in the isospin-0 channel can account for the anomalously large isospin violation effects observed by BESIII for $\eta(1407/1475)$ and $f_1(1420) \to f_0(980)\pi \to 3\pi$ [10]. A similar dynamic mechanism was suggested earlier by Achasow and Kozhevnikov [11] to explain the resonance-like signal observed in the $\phi\pi^0$ mass spectrum of the reaction $\pi^- p \to \phi\pi^0 n$ [12] by the decay of $\rho(1700) \to K^\star\bar{K}$ and rescattering of $K\bar{K} \to \phi$. Triangle singularities are currently also being discussed in the context of the newly discovered XYZ quarkonium peaks [13].

Our paper is organized as follows. In sections II to IV, we only discuss the triangle diagram for process (i) with intermediate particles $(K^{\star 0}, K^+, K^-)$, the calculation for process (ii) proceeds analogously. In section II the kinematic conditions for the appearance of the triangle singularity are analyzed. The amplitude for the triangle process is calculated in the following two sections. In section III we first present an approach to calculate the imaginary part of the amplitude making use of Cutkosky cutting rules and the calculation of discontinuities. This method helps to understand the structure of the amplitude singularities. In section IV we then use an effective Lagrangian approach [14] to calculate the full amplitude,

i.e. the real and imaginary parts, needed to predict the phase motion. In both sections, we start with the case of scalar particles to illustrate the underlying physics. In scalar theory the behavior of the amplitude is $\propto \log(s - E_1^2)$ near the singularity. Since the amplitude behavior could be different in scalar theory and in interactions of particles with spin [11], then the realistic situation for particles with spin and finite width is calculated. We show that the singularity is removed only by including the finite width of unstable particles and gives a contribution $\sim \log \Gamma_{K^\star}$.

In section V we estimate the branching ratio of $a_1(1260) \to f_0(980)\pi^-$, now including both isospin combinations, relative to its dominant decay channel $\rho\pi^-$, and compare the signal we expect for the triangle diagram to experimental values as reported in [6].

II. KINEMATIC CONDITIONS FOR TRIANGLE SINGULARITY

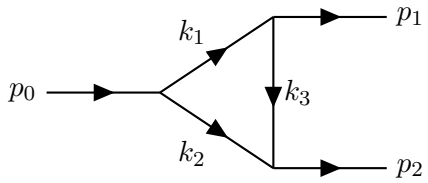

Figure 1. The process $0 \to 1 + 2$ for particles with 4-momenta p_0, p_1, p_2, proceeding via a triangle diagram with intermediate particle momenta k_1, k_2, k_3.

It is well known that logarithmic singularities arise in processes which proceed via the triangle diagram shown in Fig. 1. As it was shown by a general analysis of singularities in scalar theory [15], the amplitude behavior near the branching point of a cut is $\propto \log(s - s_0)$, where s is an external invariant. The position of the singularity s_0 can be obtained from the simple condition that all intermediate particles are on mass shell and collinear to each other. It is given by the system of Lorentz-invariant Landau equations:

$$\begin{cases} k_i^2 = m_i^2, & i = 1 \dots 3, \\ x\, k_{1\mu} - y\, k_{2\mu} + z\, k_{3\mu} = 0, & x, y, z \in [0, 1], \\ x + y + z = 1, \end{cases} \tag{1}$$

with k_i and m_i the 4-momenta and masses of intermediate particles, respectively, and x, y, z the so-called Feynman parameters. The system of equations (1) for x, y, z is overdetermined, so it is solvable only in exceptional cases. For the special case of the decay of $a_1^-(1260)$ to $f_0(980)\pi^-$ through intermediate particles $(K^{\star -}, \bar{K}^0, K^0)$ or $(K^{\star 0}, K^+, K^-)$, and neglecting the finite width of the $f_0(980)$, the external momenta p_1 and p_2 depend only on $s = p_0^2$ (see Fig. 1 for the definition of p_i). Using kinematical relations between internal and external momenta it can be shown that the system (1) has solutions only if $\sqrt{s} = E_{1,2}$, where $E_1 = 1.42\,\text{GeV}$, $E_2 = 1.46\,\text{GeV}$. These pinch singularities are shown as dots in Fig. 2. As can be seen, the conditions $x, y, z \in [0, 1]$ are satisfied only for the first solution.

Here we give a simple kinematic explanation for the appearance of the singularity. The initial state $a_1(1260)$ with $J^{PC} = 1^{++}$ can decay to real $K^\star \bar{K} + c.c.$ starting from the threshold $\sqrt{s} = 1.39\,\text{GeV}$. Then the $K^\star$ decays to real K and π. Note that the K from $K^\star$ decay can go to the same direction as the $\bar{K}$, the ratio of velocities of $\bar{K}$ and K is a function

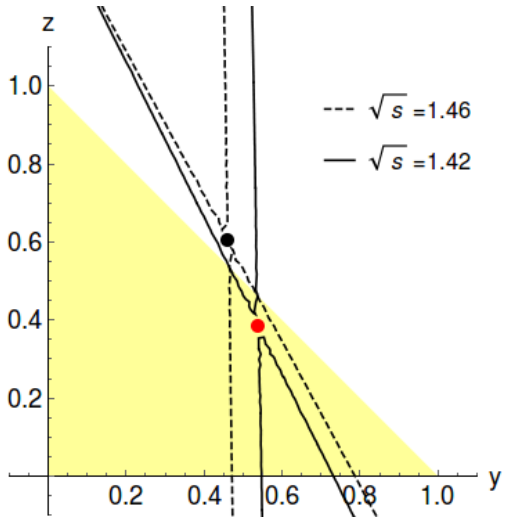

Figure 2. Diagram illustrating the positions of singularities of the triangle diagram shown in Fig. 1 for the Feynman variables y, z. The light-gray triangle is the kinematically allowed region. The black dots are pinch singularities, corresponding to $\sqrt{s} = E_1$ (lower dot) and $\sqrt{s} = E_2$ (upper dot), respectively. The curves are solutions of $\Delta_{yz} + m_1^2(1-y-z) = 0$ (see equations 16 and 17) for $\sqrt{s} = E_1$ (solid line) and $\sqrt{s} = E_2$ (dashed line).

of $\sqrt{s}$ as well as of the invariant mass of K and $\bar{K}$. The invariant mass of $\bar{K}$ K going in the same direction is equal to the mass of f_0 only if $\sqrt{s} = E_{1,2}$, but for E_2 the $\bar{K}$ is faster than K and thus the K cannot catch up the $\bar{K}$ to form f_0. Only for the solution E_1 do the K and $\bar{K}$ proceed in the same direction with the same velocity with an invariant mass equal to that of the f_0.

The kinematics discussed here demonstrates a very peculiar situation in the decay of the $a_1(1260)$ to $K^\star\bar{K} + c.c$: just above the two-body threshold, the re-scattering in the triangle can happen with particles almost on mass shell.

III. IMAGINARY PART OF THE AMPLITUDE

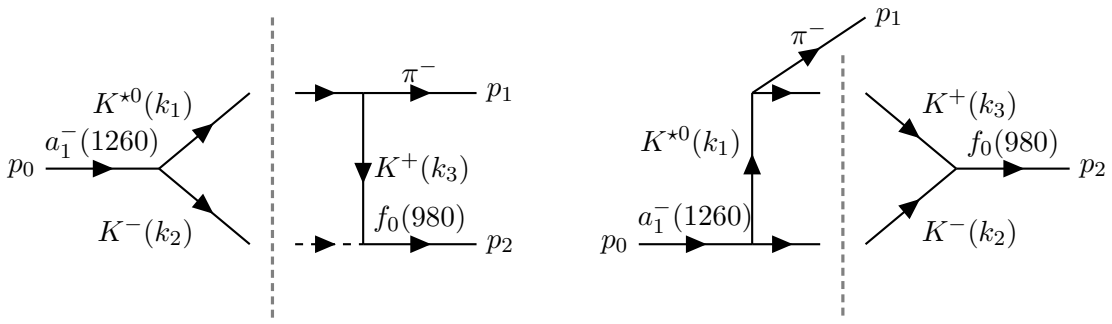

Figure 3. Two possible cuts which contribute to the imaginary part of the matrix element of the process $a_1(1260) \to f_0(980)\pi^-$.

In order to understand the structure of the amplitude, we first consider the imaginary part only, based on discontinuities. The technique was developed by Cutkosky [16], is described e.g. in the Gribov lectures [17], and was successfully applied by Achasov and Kozhevnikov for similar process, $\rho' \to \phi\pi$ [11]. The imaginary part of the amplitude $\mathbb{M}$ of the diagram in Fig. 1 is related to the discontinuity across the cuts shown in Fig. 3 by

$$\mathrm{Im}\,\mathbb{M}_{a_1\to f_0\pi} = \frac{1}{2}\left(\mathrm{Disc}_{K^\star K} + \mathrm{Disc}_{K\bar{K}}\right) \ . \tag{2}$$

To calculate the discontinuities, we use the following expression

$$\mathrm{Disc} = \int \prod_{\mathrm{cut}} \frac{\mathrm{d}^3 k_i}{(2\pi)^3 2E_i^k} \times \left(\sum_{\mathrm{polarization}} \mathbb{M}_1 \cdot \mathbb{M}_2^\star \right) \times (2\pi)^4 \delta^4(\mathrm{mom.\ cons.}) \ , \tag{3}$$

where $\mathbb{M}_{1,2}$ are matrix elements for processes on the left and right hand side of the cutting line, respectively (see Fig. 3). We are calling particles which are crossed by cut line as cut particles. The integration is over all momentum space for cut particles, i.e. k_i are momenta of cut particles, E_i^k are the corresponding energies. If a cut particle has spin we sum over all possible polarizations.

A. Simple model with scalar intermediate particles

For the case of scalar intermediate particles, the expressions for the discontinuities are:

$$\mathrm{Disc}^{(\mathrm{sc})}_{K^\star K} = g^3 \int \frac{\mathrm{d}^3 k_1}{(2\pi)^3 2E_1^k} \frac{\mathrm{d}^3 k_2}{(2\pi)^3 2E_2^k} \times \frac{1}{m_3^2 - k_3^2 + i\epsilon} \times (2\pi)^4 \delta^4(p_0 - k_1 - k_2) \ , \tag{4}$$

$$\mathrm{Disc}^{(\mathrm{sc})}_{K\bar{K}} = g^3 \int \frac{\mathrm{d}^3k_2}{(2\pi)^3 2E_2^k} \frac{\mathrm{d}^3k_3}{(2\pi)^3 2E_3^k} \times \frac{1}{m_1^2 - k_1^2 - i\epsilon} \times (2\pi)^4 \delta^4(k_3 + k_2 - p_2) \ . \tag{5}$$

Here, the products of matrix elements $\mathbb{M}_1 \cdot \mathbb{M}_2^\star$ are given by the coupling constants at the three vertices, which are set to g, and the propagator, which is a function of the angle between $\vec{k}_1$ and $\vec{p}_1$ in equation (4) and a function of the angle between $\vec{k}_2$ and $\vec{p}_1$ in equation (5). For both discontinuities, the cut particles ($K^\star$, K^- and K^+, K^-, respectively) are set on their mass shells. Integration with delta function in equation (5) is performed in the f_0 rest frame. After carrying out the integration we arrive at the following expression:

$$\mathrm{Im}\,\mathbb{M}^{(\mathrm{sc})}_{a_1 \to f_0 \pi} = \frac{g^3}{16\pi} \left[\frac{1}{2|\vec{p}|\sqrt{s}} \log \frac{\tilde{A} + 1 + i\epsilon}{\tilde{A} - 1 + i\epsilon} + \frac{1}{2|\vec{p}\,'|M_1} \log \frac{\tilde{C} + 1 - i\epsilon}{\tilde{C} - 1 - i\epsilon} \right] \ , \tag{6}$$

where the coefficients $\tilde{A}$, $\tilde{C}$ originate from the propagators,

$$\tilde{A} = (m_3^2 - m_1^2 - M_1^2 + 2E_1^p E_1^k)/(2|\vec{k}||\vec{p}\,|) \ , \tag{7}$$

$$\tilde{C} = (m_1^2 - s - m_2^2 + 2E_0' E_2^{k\prime})/(2|\vec{k}\,'||\vec{p}\,'|) \ . \tag{8}$$

Here, $M_i^2 = p_i^2$, $|\vec{k}| = \lambda^{1/2}(s, m_1^2, m_2^2)/(2\sqrt{s})$, $|\vec{p}\,| = \lambda^{1/2}(s, M_1^2, M_2^2)/(2\sqrt{s})$ are the momenta of the corresponding particles in a_1 rest frame, with the Källen function

$$\lambda(x, y, z) = x^2 + y^2 + z^2 - 2(xy + yz + zx) \ . \tag{9}$$

$E_1^k = (s + m_1^2 - m_2^2)/(2\sqrt{s})$, $E_1^p = (s + M_1^2 - M_2^2)/(2\sqrt{s})$. The values with prime are calculated at the f_0 rest frame: $|\vec{k}'| = \lambda^{1/2}(M_2^2, m_2^2, m_3^2)/(2M_2)$, $|\vec{p}\,'| = \lambda^{1/2}(s, M_1^2, M_2^2)/(2M_2)$ are the momenta of K^+ (K^-) and π^- (a_1^-). The corresponding expressions for energy are $E_2^{k\prime} = (M_2^2 + m_2^2 - m_3^2)/(2M_2)$, $E_0' = (s + M_2^2 - M_1^2)/(2M_2)$. The imaginary parts of the expressions (4), (5) compensate each other and the equation (6) is real.

The imaginary part of the amplitude $\mathrm{Im}\,\mathbb{M}^{(\mathrm{sc})}_{a_1 \to f_0 \pi}(s)$ as well as the contributions from the individual discontinuities are shown in Fig. 4 by dashed lines. One can clearly see singularity $\sqrt{s} = E_1$ and E_2 values. The singularity in E_2 is out of kinematically allowed region of reaction, so the sum of the two discontinuities is smooth at E_2. One can also notice that the imaginary part is not zero below the threshold of $K^\star K$ threshold. Here, the contribution comes from $\mathrm{Disc}_{K\bar{K}}$, because the mass m_{f_0} is above $2m_{K^\pm}$ threshold. Of course, taking into account the real shape of $K^\star$ and f_0 will make the amplitude smoother, as shown in section IV C, but the effect of the singularity at $\sqrt{s} = E_1$ will remain. This conclusion will also not change when the spin of the particles is taken into account, as will be shown in the next section.

B. Realistic case: VPP intermediate particles

In reality, the particles involved in the process carry quantum numbers different from the scalar particles used in the previous section. The $a_1(1260)$ with axial-vector quantum numbers $J^P = 1^+$ decays to $K^\star\bar{K}$ with vector and pseudoscalar quantum numbers, respectively. The $K^\star$ decays to two pseudoscalars, $K\pi$. The Feynman rules for the hadronic vertices which we use are given in appendix A.

The expressions for the discontinuities are:

$$\mathrm{Disc}^{(\mathrm{vpp})}_{K^\star\bar{K}} = g^3 \int \frac{\mathrm{d}^3k_1}{(2\pi)^3 2E_1^k} \frac{\mathrm{d}^3k_2}{(2\pi)^3 2E_2^k} \times \frac{\varepsilon_{0\mu}\left(g^{\mu\nu} - \frac{k_1^\mu k_1^\nu}{m_1^2}\right)(p_1 - k_3)_\nu}{m_3^2 - k_3^2 + i\epsilon} \times (2\pi)^4\delta^4(p_0 - k_1 - k_2), \tag{10}$$

$$\mathrm{Disc}^{(\mathrm{vpp})}_{K\bar{K}} = g^3 \int \frac{\mathrm{d}^3k_2}{(2\pi)^3 2E_2^k} \frac{\mathrm{d}^3k_3}{(2\pi)^3 2E_3^k} \times \frac{\varepsilon_{0\mu}\left(g^{\mu\nu} - \frac{k_1^\mu k_1^\nu}{m_1^2}\right)(p_1 - k_3)_\nu}{m_1^2 - k_1^2 - i\epsilon} \times (2\pi)^4\delta^4(k_3 + k_2 - p_2). \tag{11}$$

Here ε_0 is a polarization vector of the a_1 state, we use notation shown in Fig. 3.

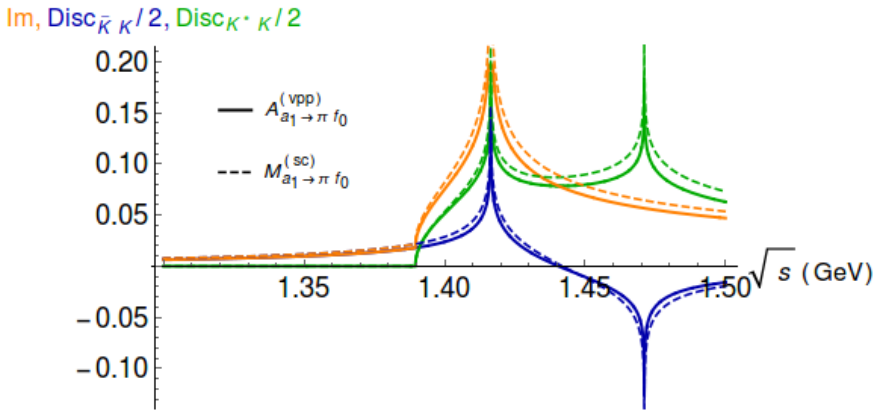

Figure 4. Energy dependence of $\mathrm{Im}\,\mathbb{M}^{(\mathrm{sc})}_{a_1\to f_0\pi}(s)$ and $\mathrm{Im}\,\mathbb{A}^{(\mathrm{vpp})}_{a_1\to f_0\pi}(s)$ (dashed and full lines, respectively). The contributions of the discontinuities $K^\star\bar{K}$ and $K\bar{K}$ are shown by green and blue lines, respectively.

After integration, we have:

$$\mathrm{Disc}^{(\mathrm{vpp})}_{K^\star\bar{K}} = g^3 \frac{1}{8\pi} \frac{2|\vec{k}|}{\sqrt{s}} (\varepsilon_0(p_1 - p_2)) \times \\ \times \frac{M_1^2 + m_1^2 - m_3^2}{4m_1^2\vec{p}_1^2} \left[1 + \left(-\frac{|\vec{p}|}{|\vec{k}|}\frac{m_1^2}{M_1^2 + m_1^2 - m_3^2} + \frac{\tilde{A}}{2}\right)\log\frac{\tilde{A} - 1 + i\epsilon}{\tilde{A} + 1 + i\epsilon}\right], \tag{12}$$

$$\mathrm{Disc}^{(\mathrm{vpp})}_{K\bar{K}} = -g^3 \frac{1}{8\pi} \frac{2|\vec{k}'|}{M_2} \left(\varepsilon_0(p_1 - p_2)\right) \times$$
$$\times \frac{M_1^2 + m_1^2 - m_3^2}{4m_1^2 \vec{p}'^2} \frac{E_0'}{M_2} \left[1 + \left(\frac{|\vec{p}'|}{|\vec{k}'|} \frac{2m_1^2 M_2 - (M_1^2 + m_1^2 - m_3^2)E_2^{k\prime}}{(M_1^2 + m_1^2 - m_3^2)E_0'} + \frac{\tilde{C}}{2}\right) \log \frac{\tilde{C} - 1 - i\epsilon}{\tilde{C} + 1 - i\epsilon}\right] \quad . \tag{13}$$

The notations could be found in the previous section. The P-wave from $K^\star$ decay is propagated to the $f_0\pi$ P-wave. So we have a factor $(\varepsilon_0(p_1 - p_2))$ in the final expression for the imaginary part of the matrix element. We separate it to compare the result with the scalar case:

$$\mathbb{M}^{(\mathrm{vpp})}_{a_1 \to f_0\pi} = g^3 \, \mathbb{A}^{(\mathrm{vpp})}_{a_1 \to f_0\pi} (\varepsilon_0(p_1 - p_2)) \quad . \tag{14}$$

$\mathbb{A}^{(\mathrm{vpp})}_{a_1 \to f_0\pi}$ is plotted in Fig. 4 together with the result from the scalar theory. The two results are very similar.

IV. FULL AMPLITUDE FOR $a_1^-(1260) \to f_0(980)\,\pi^-$ VIA $K^{\star 0}K^+K^-$ TRIANGLE

After the calculation of the imaginary part of the amplitude based on discontinuities we proceed now to the calculation of the full amplitude for the triangle diagram shown in Fig. 5 using Feynman rules for hadronic processes in an effective Lagrangian approach [14] (see appendix A for the parameterization of vertices). As in the previous section, we start from the simple case of scalar particles, and generalize to particles with spin in section IV B.

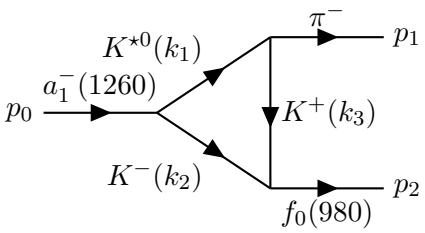

Figure 5. $a_1(1320) \to f_0(980)\pi^-$ triangle diagram.

A. Simple model with scalar intermediate particles

In case of vertices involving scalar particles only the matrix element for the triangle diagram in Fig. 5 is

$$\mathbb{M}^{(\mathrm{sc})}_{a_1\to f_0\pi} = g^3 \int \frac{\mathrm{d}^4k_1}{(2\pi)^4 i} \frac{1}{(m_1^2 - k_1^2 - i\epsilon)(m_2^2 - (p_0 - k_1)^2 - i\epsilon)(m_3^2 - (k_1 - p_1)^2 - i\epsilon)} \ , \quad (15)$$

We calculate the integral using the standard technique of Feynman parameters and Wick rotation, which is described in more detail in appendix B:

$$\mathbb{M}^{(\mathrm{sc})}_{a_1\to \pi f_0} = \frac{g^3}{16\pi^2} \int_0^1 \mathrm{d}y \int_0^{1-y} \mathrm{d}z \frac{1}{\Delta_{yz} + m_1^2(1-y-z) - i\epsilon} \ , \quad (16)$$

where Δ_{yz} is given by

$$\Delta_{yz} = y m_2^2 + z m_3^2 - y(1-y-z)p_0^2 - z(1-z-y)p_1^2 - yz p_2^2 \ . \quad (17)$$

Equation (16) is evaluated numerically and the real and imaginary parts are shown in Fig. 6 (left panel). If the widths of all intermediate particles are set to zero, the detailed structure of the amplitude becomes apparent. The imaginary part starts to grow rapidly from threshold $\sqrt{s_{\mathrm{th}}} = m_K + m_{K^\star}$ and goes to infinity when $\sqrt{s} = E_1$. It exactly reproduces our result from section III shown in Fig. 4. The real part has a cusp at the threshold, then sharply drops below zero at $\sqrt{s} = E_1$ and becomes stable for higher values of $\sqrt{s}$.

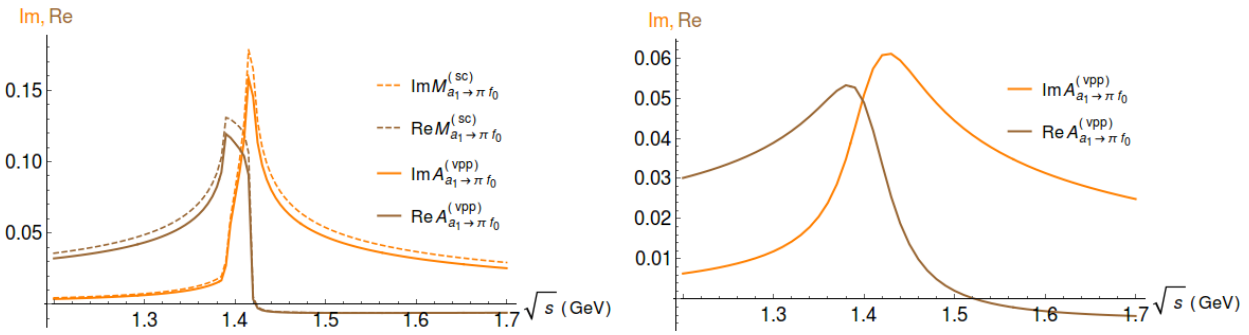

Figure 6. (Left) Real (brown) and imaginary (orange) parts of $\mathbb{A}^{(\mathrm{vpp})}_{a_1\to\pi f_0}(s)$ and $\mathbb{M}^{(\mathrm{sc})}_{a_1\to\pi f_0}(s)$, respectively. (Right) Real (brown) and imaginary (orange) parts of $\mathbb{A}^{(\mathrm{vpp})}_{a_1\to\pi f_0}(s)$ when the finite width of $K^\star$ is taken into account in VPP case.

B. Realistic case: VPP intermediate particles

For the realistic case of vector and pseudoscalar intermediate particles the expression for the matrix element is

$$\mathbb{M}^{(\mathrm{vpp})}_{a_1\to\pi f_0} = g^3 \int \frac{\mathrm{d}k_1^4}{(2\pi)^4\, i} \frac{\varepsilon_{0\mu}\left(g^{\mu\nu} - \frac{k_1^\mu k_1^\nu}{k_1^2}\right)(p_1 - k_3)_\nu}{(m_1^2 - k_1^2 - i\epsilon)(m_2^2 - (p_0 - k_1)^2 - i\epsilon)(m_3^2 - (k_1 - p_1)^2 - i\epsilon)} \quad . \tag{18}$$

We can apply the same procedure as in section IV A, introducing Feynman parameters and performing a Wick rotation, and then calculate the resulting integral numerically. The details of the calculation are shown in appendix B 0 a. Using the relation between $\mathbb{A}^{(\mathrm{vpp})}_{a_1\to\pi f_0}$ and $\mathbb{M}^{(\mathrm{vpp})}_{a_1\to\pi f_0}$ given in equation (14), the result is

$$\begin{aligned}\mathbb{A}^{(\mathrm{vpp})}_{a_1\to\pi f_0} = {} & \frac{1}{16\pi^2}\int_0^1 \mathrm{d}y \int_0^{1-y} \mathrm{d}z \frac{1}{\Delta_{yz} + m_1^2(1-y-z) - i\epsilon} + \\ & + \frac{1}{16\pi^2}\int_0^1 \mathrm{d}y \int_0^{1-y} \mathrm{d}z \int_0^{1-y-z} \mathrm{d}x \left(\frac{yz(p_0\cdot p_1) + z^2 p_1^2}{(\Delta_{yz} + m_1^2 x - i\epsilon)^2} - \frac{1/4}{\Delta_{yz} + m_1^2 x - i\epsilon}\right) \quad . \end{aligned} \tag{19}$$

The real and imaginary parts of $\mathbb{A}^{(\mathrm{vpp})}_{a_1\to\pi f_0}$ are compared to the scalar case in Fig. 6 (left). For both real and imaginary parts, the result for the VPP case is very similar to the scalar one, as was already shown for the imaginary part in section III.

C. Corrections to $K^\star \to K\pi$ vertex

There are two additional corrections to be taken into account in order to arrive at a realistic estimate of the triangle amplitude:

1. Finite widths of intermediate particles. Until now we have assumed that the particles in the loop are stable ($\epsilon \to 0$). While this is reasonable for K, the width of $K^\star$ is $\Gamma_{K^\star} = 0.05\,\mathrm{GeV}$,

2. P-wave tail suppression. In the VPP case the $K^\star$ decays to $K\pi$ in a P-wave, which is propagated to the $f_0\pi$ final state, $\left|\mathbb{M}^{(\mathrm{vpp})}_{a_1\to\pi f_0}\right|^2 \sim \left(\mathbb{A}^{(\mathrm{vpp})}_{a_1\to\pi f_0}\right)^2 |\vec{p}_\pi|^2$, ($|\vec{p}_\pi|$ is $a_1 \to f_0\pi$ break up momentum). Therefore, the final f_0 and π effectively are in a P-wave. This gives rise to an enhanced, unphysical tail in the signal intensity.

To take into account the finite width of intermediate particles we substitute propagators of stable particles by resonance propagators. Technically this leads to substitutions $m_j^2 \to m_j^2 - im_j\Gamma_j$. Including such a term for the $K^\star$ propagator in equation (18) results in a smoother behavior of the amplitude, as shown in Fig. 6 (right panel). The singularity at $\sqrt{s} = E_1 = 1.42\,\mathrm{GeV}$ is now limited and proportional to $\log\Gamma_{K^\star}$.

For a two-body decay with orbital angular momentum L, the amplitude behaves like p^L close to threshold due to centrifugal barrier. Far away from threshold, this is no longer correct because of the finiteness of the strong interaction. Accounting for the finiteness of interaction, however, is not unique. For a direct decay of a resonance phenomenological form factors are usually used, which come from a classical potential model. These could be Blatt-Weisskopf barrier factors [18] or exponential factors for finite meson-size corrections [19]. Another phenomenological approach is to introduce a simple left-hand singularity in the amplitude as a vertex form factor [20]. We demonstrate here that the latter approach, where a pole is introduced in the amplitude to account for the $K^\star$ P-wave decay, gives a reasonable result. To do so, we include in equation (18) a factor

$$F(k_1) = \frac{C}{M^2 - k_1^2} \tag{20}$$

under the integral, where M is the position of the left-hand singularity and C is a constant normalized to the $K^\star \to K\pi$ decay from mass shell, $C = M^2 - m^2_{K^\star}$. Above the $K\pi$ threshold this correction behaves like a D-wave Blatt-Weisskopf factor ($F^{(D)}_{\mathrm{bw}}$). So M corresponds to the size of $K^\star$

$$F^{(D)}_{\mathrm{bw}}(\vec{p})^{-1/2} \sim 1 + R^2|\vec{p}|^2 \approx 1 + R^2\frac{(k_1^2 - (m_\pi + m_K)^2)(k_1^2 - (m_\pi - m_K)^2)}{4k_1^2} \approx$$
$$\approx 1 + R^2\frac{(k_1^2 - (m_\pi + m_K)^2)}{4} = -\frac{R^2}{4}(M^2 - k_1^2), \quad M^2 = (m_\pi + m_K)^2 - \frac{4}{R^2}\ . \tag{21}$$

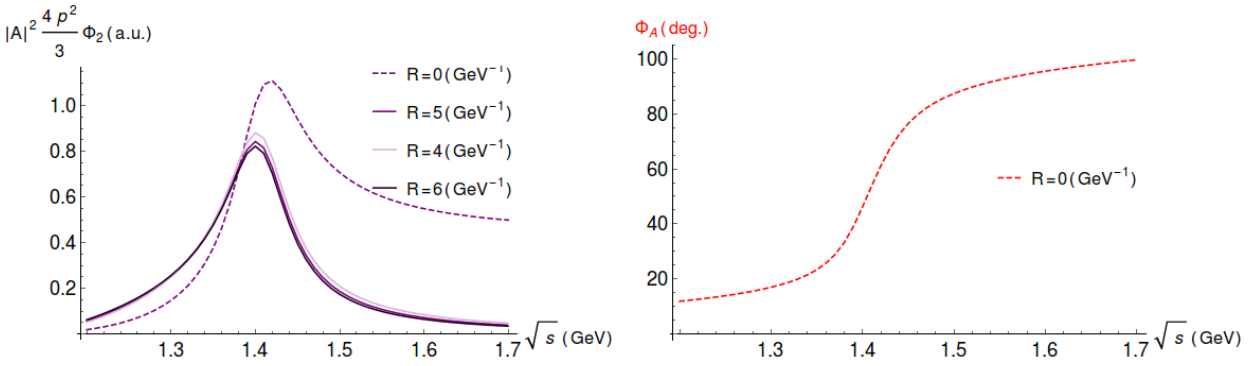

Figure 7. The intensity (left side) and the phase (right side) of the final amplitude $\mathbb{A}_{a_1\to\pi f_0}(s)$ including finite width of $K^\star$ and P-wave tail suppression (see equation (19)) as a function of $\sqrt{s}$ for different values of the suppression parameter R.

With this form of correction, our standard approach of Feynman parameters and Wick rotation can be used; the details of the calculation are again moved to appendix B. The final expression is

$$\mathbb{A}^{(\mathrm{vpp})}_{a_1\to f_0\pi} \to \frac{C}{16\pi^2}\int_0^1 \mathrm{d}y \int_0^{1-y} \mathrm{d}z \times \left(\frac{(1-y-z)}{(\Delta_{yz}+m_1^2(1-y-z))(\Delta_{yz}+M^2(1-y-z))} + \frac{(z^2p_1^2+yz(p_1\cdot p_2))(1-y-z)^2}{(\Delta_{yz}+m_1^2(1-y-z))\times(\Delta_{yz}+M^2(1-y-z))\times\Delta_{yz}} - \frac{1}{4}\frac{2}{M^2}\left[\frac{1}{m_1^2}\log\frac{\Delta_{yz}+m_1^2(1-y-z)}{\Delta_{yz}} - \frac{1}{m_1^2-M^2}\log\frac{\Delta_{yz}+m_1^2(1-y-z)}{\Delta_{yz}+M^2(1-y-z))}\right]\right) . \quad (22)$$

The final result including the final width of $K^\star$ and the suppression of the P-wave tail at higher energies is plotted in Fig. 7. The left panel shows the intensity, $|\mathbb{A}_{a_1\to\pi f_0}|^2\,(4p^2/3)\;\Phi_2$, where Φ_2 is the two-body phase space, for different values of the size parameter $R = 0.8-1.2\,\mathrm{fm}$, and also without suppression ($R=0$). The tail is indeed suppressed as expected, almost independent of the exact value of R. The phase of the signal for $R=0$ (no suppression) is shown in the right panel.

Including the suppression factor in the integral of equation (18) artificially shifts the phase to lower values with respect to the case with no suppression. The phase motion, i.e. the relative difference as a function of the energy is not affected. Therefore we show only the phase for $R=0$.

V. THE REACTION $\pi^- p \to a_1^-(1260) p \to f_0(980)\pi^- p$

A. Cross section

With a high-energy pion beam, as used in COMPASS and VES, the $a_1^-(1260)$ is produced in a diffractive process proceeding via t-channel Pomeron exchange between the beam π^- and the target proton, as shown in Fig. 8.

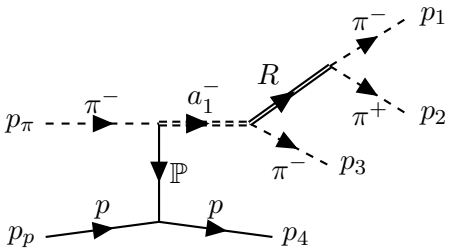

Figure 8. Diagram for diffractive production of the $a_1(1260)$ by scattering of a high-energy π^- off a proton target, which remains intact. The $\pi^-\pi^+\pi^-$ final state observed in the experiment is modeled by the decay of the a_1^- into a charged pion and a neutral isobar R (ρ^0 or $f_0(980)$), which subsequently decays into two charged pions. The isobar can be formed either by $\pi_1^-\pi_2^+$ or by $\pi_2^+\pi_3^-$.

In order to estimate the intensity of the signal expected in the $f_0(980)\pi^-$ channel we calculate its intensity and phase difference compared to the dominant $a_1^-(1260) \to \rho^0\pi^-$ decay, assuming that the signal in $f_0\pi^-$ is entirely due to the triangle singularity in the decay $a_1^-(1260) \to f_0(980)\pi^-$. We denote the invariant mass squared of the a_1 by s, and the isobar invariant mass squared by s_{12} or s_{23}, respectively. Factorizing out the production cross section $\sigma_{\text{prod}}(s)$ of the $a_1(1260)$, which is independent of the final state, the differential cross section for the full process $\pi^- p \to a_1^-(1260)p \to R\,\pi^- p \to \pi^-\pi^+\pi^- p$ can be written as

$$\frac{\mathrm{d}\sigma}{\mathrm{d}s} = \frac{\sigma_{\text{prod}}(s)}{4\pi}\left[\int \frac{\mathrm{d}s_{12}}{2\pi}\frac{2m_{a_1}\Gamma_{a_1^-\to R\pi^-}(s,s_{12})}{(m_{a_1}^2-s)^2+m_{a_1}^2\Gamma_{a_1}^2(s,s_{12})}\frac{2m_R\Gamma_{R\to\pi^+\pi^-}(s_{12})}{(m_R^2-s_{12})^2+m_R^2\Gamma_R^2(s_{12})}+ \right.$$
$$\left. +\{12\leftrightarrow 23\}+\int \mathrm{d}\Phi_{3\pi}\,\mathrm{Interf}(s_{12},s_{23})\right] \quad , \quad (23)$$

where $\Gamma_{a\to bc}$ is the partial width for the two-body decay $a \to bc$, $m_{a_1,R}$ and $\Gamma_{a_1,R}$ are the pole masses and mass-dependent full widths of a_1 and R, respectively, and $\mathrm{d}\Phi_{3\pi}$ is the 3π phase space. The first two terms constitute the contributions with the isobar in the $\pi_1^-\pi_2^+$ and in the $\pi_2^+\pi_3^-$ subsystem, respectively. The third term is the contribution of the interference

between two processes. The latter is found to be very small for $a_1^- \to \rho^0\pi^-$ (less then 2% for a_1 decay from its mass shell) as well as for $a_1^- \to f_0\pi^-$, so we will disregard that contribution and use the following equation for the cross section:

$$\frac{\mathrm{d}\sigma}{\mathrm{d}s} \approx \frac{\sigma_{\mathrm{prod}}(s)}{2\pi} \int \frac{\mathrm{d}s_{12}}{2\pi} \frac{2m_{a_1}\Gamma_{a_1^-\to R\pi^-}(s,s_{12})}{(m_{a_1}^2-s)^2+m_{a_1}^2\Gamma_{a_1}^2(s,s_{12})} \frac{2m_R\Gamma_{R\to\pi^+\pi^-}(s_{12})}{(m_R^2-s_{12})^2+m_R^2\Gamma_R^2(s_{12})} \ . \tag{24}$$

The partial widths of a_1 and isobar decays are calculated by averaging the expressions for the square of the matrix elements of the corresponding hadronic vertices over the initial states and summing over the final ones and multiplying by the corresponding phase space. For the decay $a_1^-(1260) \to \rho^0\pi^-$ (axial vector to vector and pseudoscalar, AVP), we have

$$\Gamma_{a_1^-\to\rho^0\pi^-}(s,m^2) = \frac{1}{2m_{a_1}} g^2_{a_1^-\rho^0\pi^-} \left[1+\frac{|\vec{p}_\rho|^2}{3m^2}\right] \times \frac{1}{8\pi}\frac{2|\vec{p}_\rho|}{\sqrt{s}} \ , \tag{25}$$

while for $a_1^-(1260) \to f_0\pi^-$ (axial vector to pseudoscalar and scalar, APS), we get

$$\Gamma_{a_1^-\to f_0\pi^-}(s,m^2) = \frac{1}{2m_{a_1}} g^2_{a_1^- f_0\pi^-}(s,m^2) \frac{4|\vec{p}_{f_0}|^2}{3} \times \frac{1}{8\pi}\frac{2|\vec{p}_{f_0}|}{\sqrt{s}} \ , \tag{26}$$

where $|\vec{p}_{\rho/f_0}(s,m^2)| = \lambda^{1/2}(s,m^2,m_\pi^2)/(2\sqrt{s})$ is the break-up momentum for the two-body decay of a particle with mass $\sqrt{s}$ to particles with masses $m = \sqrt{s_{12}}$ and m_π. The coupling of a_1^- to $f_0\pi^-$ in equation (26) is given by

$$g^2_{a_1^- f_0\pi^-}(s,m^2) = \left|\mathbb{A}^{(\mathrm{vpp})}_{a_1\to f_0\pi}\right|^2 \left(g^{(K^\star\bar{K}+c.c.)}_{a_1^- f_0\pi^-}\right)^2 \ , \tag{27}$$

where $\mathbb{A}^{(\mathrm{vpp})}_{a_1\to f_0\pi}$ is the triangle amplitude calculated in equation (22) and $g^{(K^\star\bar{K}+c.c.)}_{a_1^- f_0\pi^-}$ is an effective coupling which includes the couplings of the individual vertices in the triangle diagram, taking into account both isospin channels.

The expressions for the isobar decays are

$$\Gamma_{\rho^0\to\pi^+\pi^-}(m^2) = \frac{1}{2m_\rho} g^2_{\rho^0\pi^+\pi^-} \frac{4|\vec{p}_\pi|^2}{3} \times \frac{1}{8\pi}\frac{2|\vec{p}_\pi|}{m} \ , \tag{28}$$

and

$$\Gamma_{f_0\to\pi^+\pi^-}(m^2) = \frac{1}{2m_{f_0}} \frac{2}{3} g^2_{f_0\pi\pi} \times \frac{1}{8\pi}\frac{2|\vec{p}_\pi|}{m} \approx \frac{2}{3}\bar{g}_{f_0\pi\pi}|\vec{p}_\pi| \ , \tag{29}$$

where the dimensionless coupling $\bar{g}_{f_0\pi\pi} = g^2_{f_0\pi\pi}/(8\pi m^2_{f_0})$ has been introduced, and $|\vec{p}_\pi| = \lambda^{1/2}(m^2,m_\pi^2,m_\pi^2)/(2m)$ is the break-up momentum of the isobar with mass m to two pions.

B. Evaluation of the couplings

To evaluate the magnitude of $a_1 \to f_0\pi$ decay with respect to $a_1 \to \rho\pi$ S-wave we take into account two possible isospin configurations of intermediate states ($K^{\star 0}K^-K^+$) and ($K^{\star -}K^0\bar{K}^0$) and evaluate the corresponding couplings. The table gives the couplings and Clebsch-Gordan coefficients for each vertex inside the loop of the two isospin configurations.

Vertex	$K^{\star 0}K^-K^+$	$K^{\star -}K^0\bar{K}^0$
a_1^-	$g_{a_1K^\star\bar{K}}$	$g_{a_1K^\star\bar{K}}$
π^-	$\sqrt{2/3}\, g_{K^\star K\pi}$	$\sqrt{2/3}\, g_{K^\star K\pi}$
f_0	$\sqrt{1/2}\, g_{f_0K\bar{K}}$	$\sqrt{1/2}\, g_{f_0K\bar{K}}$

Since the isospin structure of both configurations is identical, the two diagrams add up. Disregarding the mass difference between charged and neutral kaons, the contributions of both are the same, so the effective coupling of process can be written as

$$g^{(K^\star\bar{K}+c.c.)}_{a_1^-f_0\pi^-} = \frac{2}{\sqrt{3}} g_{a_1K^\star K}\, g_{K^\star K\pi}\, g_{f_0K\bar{K}} \ . \tag{30}$$

We first consider a_1 decays. The resonance is rather wide, so the energy dependence of the width should be taken into account. The best knowledge about a_1 decay channels and branching ratio comes from hadronic τ decay measurements [19, 21, 22]. For simplicity we consider only the main contribution to the energy dependence of the width, which comes from $a_1 \to \rho\pi$ S-wave.

$$\Gamma_{a_1}(s) = \Gamma_{a_1}(m^2_{a_1}) \frac{|\vec{p}(s)|}{|\vec{p}(m^2_{a_1})|} \frac{m_{a_1}}{\sqrt{s}}, \quad |\vec{p}(s)| = \frac{\lambda^{1/2}(s, m^2_\rho, m^2_\pi)}{2\sqrt{s}} \ . \tag{31}$$

We use the measured branching ratios, $\mathrm{Br}(a_1 \to \rho\pi,\, S-\mathrm{wave}) \approx 60\%$, $\mathrm{Br}(a_1 \to K^\star\bar{K} + c.c.,\, S-\mathrm{wave}) \approx 2.2\%$ to extract the ratio of couplings. The ratio $g_{a_1\rho\pi}/g_{a_1K^\star\bar{K}}$ is calculated with the help of equation (24), where the energy dependence of the production mechanism is disregarded. For $a_1 \to \rho\pi$, a size correction form factor $\exp(-R^2|\vec{p}_\rho\,|^2)$, where $\vec{p}_\rho$ the is break up momentum, is applied [19]. For $R > 0.5\,\mathrm{GeV}^{-1}$, the convergence of the integral over ds in equation (24) is achieved for an upper limit of the integration $\leq 5\,\mathrm{GeV}$, while for $R = 0$ a higher limit is required. Varying R between 0 and $5\,\mathrm{GeV}^{-1}$, and including the uncertainty due to the slow convergence for $R = 0$, the resulting ratio of the couplings is

$$\frac{g^2_{a_1\rho\pi}}{g^2_{a_1K^\star\bar{K}}} = \frac{2g^2_{a_1^-\rho^0\pi^-}}{g^2_{a_1^-K^{\star 0}K^-} + g^2_{a_1^-K^{\star -}K^0}} \approx 6 - 10 \ . \tag{32}$$

For the evaluation of relative strength of $f_0\pi$ signal in section V C, we use $g^2_{a_1\rho\pi}/g^2_{a_1K^\star\bar{K}} = 6$.

The width of $K^\star$ is measured precisely and the branching to $K\pi$ P-wave is 100% [1]. The corresponding coupling can thus be extracted from

$$\Gamma_{K^\star} = \frac{1}{2m_{K^\star}}\, g^2_{K^\star K\pi}\frac{4|\vec{k}|^2}{3} \times \frac{1}{8\pi}\frac{2|\vec{k}|}{m_{K^\star}}, \quad |\vec{k}| = \lambda^{1/2}(s, m^2_{K^\star}, m^2_\pi)/(2m_{K^\star}) \tag{33}$$

to be $g^2_{K^\star K\pi} = 31.2$.

The parameterization of the f_0 is not trivial, since both decay channels ($f_0 \to 2\pi$, $f_0 \to 2K$) need to be taken into account. We make use of the Flatté parameterization [23] of the f_0 propagator and the decay width in equation (24),

$$\frac{2m_{f_0}\,\bar{g}_{\pi\pi}|\vec{p}_\pi|}{\left|m^2_{f_0} - s_{12} - im_{f_0}(\bar{g}_{\pi\pi}|\vec{p}_\pi| + \bar{g}_{K\bar{K}}|\vec{p}_K|)\right|^2}, \quad \left|\vec{p}_{\pi/K}(s_{12})\right| = \frac{1}{2}\sqrt{s_{12} - 4m^2_{\pi/K}}\ . \tag{34}$$

The measurements of the branching ratio $\mathrm{Br}(f_0 \to K\bar{K})/\left(\mathrm{Br}(f_0 \to \pi\pi)\right)$ and the ratio of couplings extracted therefrom, $R_{K/\pi} = g^2_{f_0K\bar{K}}/g^2_{f_0\pi\pi} = \bar{g}_{f_0K\bar{K}}/\bar{g}_{f_0\pi\pi} \approx 4$, are rather consistent with each other [24, 25]. But the absolute values of the couplings are not known very well. For our estimation of the branching we use $g_{f_0\pi\pi} = 2.3\,\mathrm{GeV}$ [26], so $\bar{g}_{f_0\pi\pi} = 0.21$, $\bar{g}_{f_0K\bar{K}} \approx 0.8$.

C. Evaluation of the branching ratio

The cross section calculated with the help of equation (24) for $a_1^-(1260) \to f_0\pi^- \to \pi^-\pi^+\pi^-$ is compared to the one for the dominant channel $a_1^-(1260) \to \rho^0\pi^- \to \pi^-\pi^+\pi^-$ in Fig. 9. Here, the peak of $a_1 \to \rho\pi$ has been normalized to 1, the $f_0\pi$ channel is shown in relative scale. Under the assumptions detailed in the previous subsection for the couplings, the peak-to-peak ratio is $\approx 1:100$, in very good agreement with the experimental result.

Let us discuss how reliable our estimation is and which factors could affect the magnitude and the shape of $f_0\pi$ peak. First of all, we assumed that the origin of both $K^\star\bar{K}$, which are rescattered to $f_0\pi$, and $\rho\pi$ is decay of the $a_1(1260)$ resonance. In a hadron fixed-target experiment like COMPASS or VES, however, there may be other processes which contribute to the same final state, e.g. non-resonant Deck-like processes [27]. We expect a rather large contribution of Deck-like background to $\rho\pi$ S-wave signal [27] as well as to $K^\star\bar{K}$ channel [28]. Taking into account these processes, the resulting ratio of couplings could be different from equation (32).

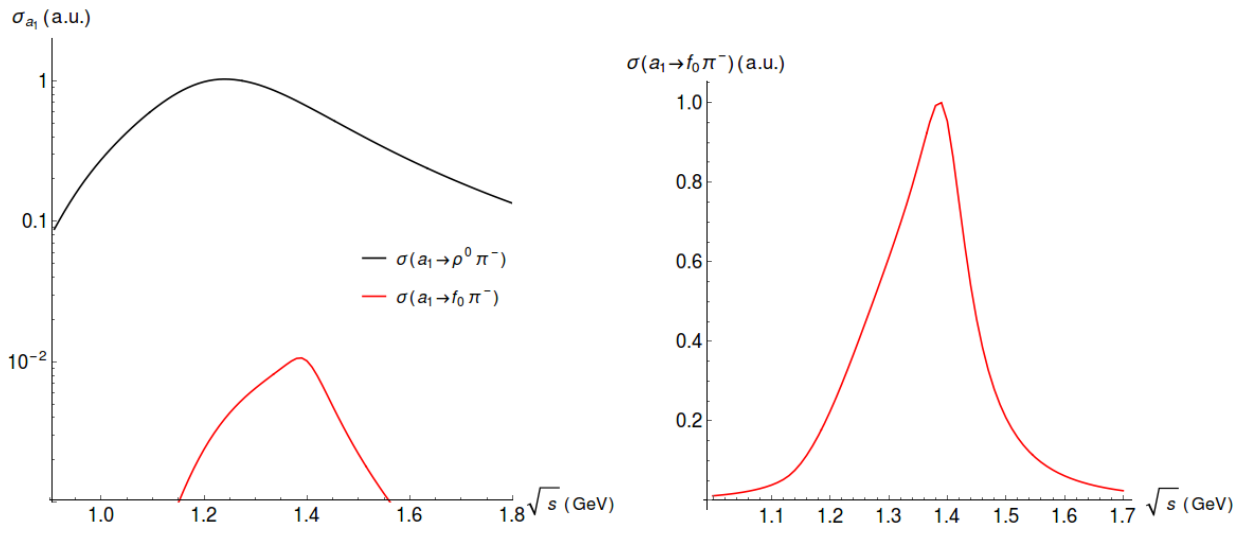

Figure 9. Cross sections for $a_1(1260)$ resonance as a function of invariant mass $\sqrt{s}$ in arbitrary units. (Left) comparison of dominant $a_1^- \to \rho^0\pi^-$ S-wave decay and $a_1^- \to f_0\pi^-$ P-wave channel due to rescattering of kaons. (Right) Pseudo-resonant shape of $a_1^- \to f_0\pi^-$ in linear scale.

Secondly, $\rho\pi \to f_0\pi$ rescattering plays an important role. Using the same method as in section IV B one can show that the triangle diagram $a_1 \to \rho\pi \to f_0\pi$ gives a rather flat amplitude with a constant phase (magnitude $\approx 4\%$ of peak intensity of $K^\star\bar{K} + c.c. \to f_0\pi$). It interferes with the signal from $K^\star\bar{K} + c.c.$ and changes its intensity and phase. Taking into account this contribution is in principle possible, but requires the knowledge of the relative sign between $a_1 \to \rho\pi$ and $a_1 \to K^\star\bar{K}$, i.e. the relative sign of $s\bar{s}$ in a_1, which is unknown.

The third uncertainty comes from the shape of the f_0 and the corresponding coupling constants. We found that the shape of our signal is stable for different values of $g_{f_0\pi\pi}$ and $R_{K/\pi}$. The relative intensity, however, is proportional to $g^2_{f_0\pi\pi}R_{K/\pi}$, which could therefore easily change by a factor of two depending on the input values.

VI. CONCLUSIONS

Even after many years of intense studies, both experimentally and theoretically, the excitation spectrum of hadrons is still not understood. This is especially true in the region of charm and bottom quarks, but also the light-quark sector sometimes bears surprises.

Present-day experiments are collecting extremely large event samples, with allow them to perform analyses with very small statistical uncertainties and permit them to find small signals which were not observable before. Recently, the COMPASS experiment has reported the observation of a resonance-like signal with axial-vector quantum numbers $J^{PC} = 1^{++}$ in a completely unexpected mass region only about 0.2 GeV above the ground state $a_1(1260)$, decaying to $f_0(980)\pi$.

In this paper we show that a resonance-like signal with a maximum intensity at 1.4 GeV, compatible with the experimental result, can be generated dynamically via a triangle singularity in the decay of the ground state $a_1(1260)$ to $K^\star\bar{K}$ + c.c and the subsequent rescattering of the K from $K^\star$ decay to form $f_0(980)$. This process also generates a rather sharp phase motion, which is not locked to the phase of the wide $a_1(1260)$. The singularity appears in a kinematic region where the intermediate particles are collinear and on mass shell. The structure of the amplitude is investigated in two ways: first, the imaginary part is calculated using cutting rules; second, the full amplitude is evaluated using Feynman rules in order to obtain the imaginary and real parts. Both approaches are performed for the hypothetical case of scalar intermediate particles and for the realistic case of vector and pseudoscalar intermediate particles. It is shown that both cases give very similar results. For the final result of the triangle amplitude, we also include the finite width of the $K^\star$ and a phenomenological factor to suppress the tail due to the P-wave decay of the $K^\star$ at high energies. The inclusion of this factor, however, is not unique, and also spoils the beauty of the solution somewhat, because it shifts the phase of the amplitude which is questionable and needs future investigation. The treatment of decays with higher angular momenta inside loops in terms of analytical solutions certainly needs more attention in the future.

We then estimate the magnitude of the signal expected in the $f_0(980)\pi$ channel due to the triangle singularity compared to the dominant decay of the $a_1(1260)$ to $\rho\pi$, also observed in the experiment. Our result gives a relative peak intensity of 1% for the $f_0\pi$ channel, with a rather large uncertainty which is due partly to poorly known couplings and partly

to other rescattering processes like $a_1 \to \rho\pi \to f_0\pi$. The last process does not produce a singularity in the kinematically allowed region, but the corresponding amplitude interferes with the $K^\star\bar{K}$ amplitude and modifies its intensity and phase. In addition, we only consider the genuine $a_1(1260)$ resonance as source for the triangle diagram, while it is known that in the reaction $\pi^- p \to 3\pi\, p$ there is a rather large contribution to the intensity in the $\rho\pi$ channel from non-resonant processes like the Deck effect, which may influence the relative branching ratio.

The dynamical interpretation of the $a_1(1420)$ presented in this paper captures the main effect and probably accounts for a large fraction of the signal observed by COMPASS and VES. As a next step, one may fit our amplitude to the data and compare to the Breit-Wigner fit, and eventually extract better values for the coupling constants. The data sample on the a_1 from τ-decays should also be large enough to observe the $f_0\pi$ peak if the data is fitted without phase locking of $f_0\pi$ with a_1. In general, the large data samples available nowadays both for light and heavy hadrons allow us to revisit effects which were already discussed more than 30 years ago, but were almost forgotten since then because data were too scarce to test them. These may play an important role in our understanding of the hadron spectrum.

ACKNOWLEDGMENTS

This work is supported by German Bundesministerium für Bildung und Forschung as well as RNF grant $\#14-22-00281$. The authors would like to thank E.L. Berger for valuable discussions during Hadron2013, and especially Q. Zhao and A.M. Zaitsev for independently pointing our attention to a triangle singularity as possible origin of the observation, and thus triggering the present work. We also thank the COMPASS Collaboration and in particular D.I. Ryabchikov for numerous discussions on the COMPASS and VES data.

Appendix A: Parameterization of vertices and Feynman rules.

First we mention the approach we use to parameterize the vertices for interactions of particles. From symmetry considerations the Lorentz structure for vertices is the following (we use S = scalar, P = pseudoscalar, V = vector, A = axial vector):

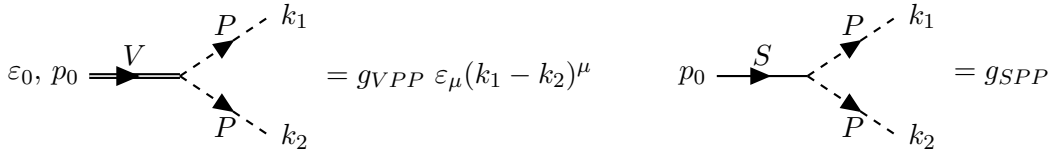

Figure 10. Parameterization of VPP vertex (P-wave) and SPP vertex (S-wave)

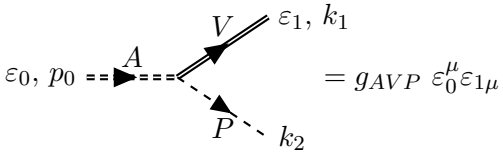

Figure 11. Parameterization of AVP vertex (S-wave)

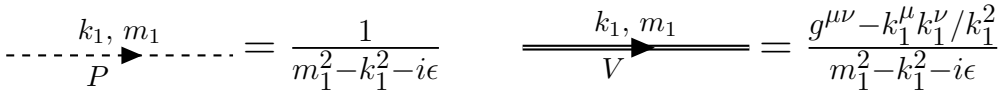

Figure 12. Propagators for pseudoscalar and vector particles

Appendix B: Calculation of integrals

In this section we calculate three integrals:

$$V_3 = \int \frac{\mathrm{d}k_1^4}{(2\pi)^4\, i} \frac{1}{\Delta_1 \Delta_2 \Delta_3}, \tag{B1}$$

$$V_4 = \int \frac{\mathrm{d}k_1^4}{(2\pi)^4\, i} \frac{\varepsilon_{0\mu} \left(g^{\mu\nu} - \frac{k_1^\mu k_1^\nu}{k_1^2} \right) (p_1 - k_3)_\nu}{\Delta_1 \Delta_2 \Delta_3}, \tag{B2}$$

$$V_5 = \int \frac{\mathrm{d}k_1^4}{(2\pi)^4\, i} \frac{\varepsilon_{0\mu} \left(g^{\mu\nu} - \frac{k_1^\mu k_1^\nu}{k_1^2} \right) (p_1 - k_3)_\nu \times \frac{C}{M^2 - k_1^2}}{\Delta_1 \Delta_2 \Delta_3}. \tag{B3}$$

where $\Delta_1 = m_1^2 - k_1^2 - i\epsilon$, $\Delta_2 = m_2^2 - (p_0 - k_1)^2 - i\epsilon$, $\Delta_3 = m_3^2 - (k_1 - p_1)^2 - i\epsilon$.

a. First integral

For the calculation of V_3, Feynman parameters (x, y, z) are introduced to rewrite the integral:

$$V_3 = \int_0^1 \int_0^1 \int_0^1 \mathrm{d}x\,\mathrm{d}y\,\mathrm{d}z\; 2!\,\delta(x+y+z-1) \int \frac{\mathrm{d}^4k}{(2\pi)^4\,i} \frac{1}{D^3} \quad , \tag{B4}$$

where $D = x(m_1^2 - k_1^2 - i\epsilon) + y(m_2^2 - (p_0 - k_1)^2 - i\epsilon) + z(m_3^2 - (k_1 - p_1)^2 - i\epsilon)$. The quadratic form $D(k_1)$ can be reduced to diagonal form collecting terms with k_1 and extracting the full square. The condition $x + y + z = 1$ is used.

$$D = -(k_1 - yp_0 - zp_1)^2 + \Delta - i\epsilon, \tag{B5}$$

$$\Delta = xm_1^2 + \Delta_{yz}, \quad \Delta_{yz} = ym_2^2 + zm_3^2 - y(1-y-z)p_0^2 - z(1-z-y)p_1^2 - yzp_2^2. \tag{B6}$$

After shifting the variable of integration $k_1 \to l = k_1 - yp_0 - zp_1$ we have

$$V_3 = \int_0^1 \int_0^1 \int_0^1 \mathrm{d}x\,\mathrm{d}y\,\mathrm{d}z\; 2!\,\delta(x+y+z-1) \int \frac{\mathrm{d}^4l}{(2\pi)^4\,i} \frac{1}{(-l^2 + \Delta - i\epsilon)^3} \quad . \tag{B7}$$

For the integration over l_0, notice that the denominator has poles when $l_0^2 = \vec{l}^2 + \Delta^2 - i\epsilon$. The positions of the poles are functions of the external invariants p_0^2, p_1^2, p_2^2 and the Feynman parameters. The basic idea, which we use is aimed to calculate the integral in the region where $p_0^2 < 0$, $p_1^2 < 0$, $p_2^2 < 0$, i.e. $\Delta > 0$ for all value of x, y, z. In that region we can rotate the contour of integration over l_0 anticlockwise (Wick rotation) and integrate along the imaginary axis. We make use of the transfer of the integration variable l to Euler space with integration variable l_E ($l^2 = -l_E^2$), where the integration is much simpler. One has:

$$V_3 = \int_0^1 \int_0^1 \int_0^1 \mathrm{d}x\,\mathrm{d}y\,\mathrm{d}z\; 2!\,\delta(x+y+z-1) \int \frac{\mathrm{d}^4l_E}{(2\pi)^4} \frac{1}{(l_E^2 + \Delta - i\epsilon)^3}. \tag{B8}$$

The next step is integration over l_E. As a result we have:

$$V_3 = \frac{1}{16\pi^2} \int_0^1 \mathrm{d}y \int_0^{1-y} \mathrm{d}z \frac{1}{\Delta_{yz} + m_1^2(1-y-z) - i\epsilon}. \tag{B9}$$

Equation (B9) is simple enough for numerical integration.

b. Second integral

Let us consider integral V_4, equation (B2). The numerator can be simplified as

$$\varepsilon_{0\mu}\left(g^{\mu\nu} - \frac{k_1^\mu k_1^\nu}{k_1^2}\right)(p_1 - k_3)_\nu = \varepsilon_{0\mu}\left(g^{\mu\nu} - \frac{k_1^\mu k_1^\nu}{k_1^2}\right)(2p_1 - k_1)_\nu = 2(\varepsilon_0 \cdot p_1) + 2\frac{(\varepsilon_0 \cdot k_1)(k_1 \cdot p_1)}{-k_1^2}. \tag{B10}$$

One can notice that k_1^2 in the numerator has the same form as $\Delta_0 = m_0^2 - k_1^2$ with mass $m_0^2 = 0$. The integral in equation (B2) is equal to

$$\frac{1}{2}V_4 = (\varepsilon_0 \cdot p_1) \int \frac{\mathrm{d}^4 k_1}{(2\pi)^4\, i} \frac{1}{\Delta_1 \Delta_2 \Delta_3} + \int \frac{\mathrm{d}^4 k_1}{(2\pi)^4\, i} \frac{(\varepsilon_0 \cdot k_1)(k_1 \cdot p_1)}{\Delta_0 \Delta_1 \Delta_2 \Delta_3}. \tag{B11}$$

The first integral in equation (B11) is equal to equation (B9). For the second one we introduce four Feynman parameters:

$$\int \frac{\mathrm{d}^4 k_1}{(2\pi)^4\, i} \frac{(\varepsilon_0 \cdot k_1)(k_1 \cdot p_1)}{\Delta_0 \Delta_1 \Delta_2 \Delta_3} = \int_0^1 \mathrm{d}t \int_0^1 \mathrm{d}x \int_0^1 \mathrm{d}y \int_0^1 \mathrm{d}z\, 3!\, \delta(t + x + y + z - 1) \int \frac{\mathrm{d}^4 k_1}{(2\pi)^4\, i} \frac{(\varepsilon_0 \cdot k_1)(k_1 \cdot p_1)}{D_4^4}, \tag{B12}$$

where for D_4 with condition $x_0 + x_1 + x_2 + x_3 = 1$ we have the same expression as equation (B5). So the same shift of the integration variable k_1 is used, i.e. $k_1 \to l = k_1 - y p_0 - z p_1$.

The expression in the numerator can be written as

$$(\varepsilon_0 \cdot k_1)(k_1 \cdot p_1) = l_\mu l_\nu \cdot \left[\varepsilon_0^\mu p_1^\nu\right] + l_\mu \cdot \left[(z p_1^2 + y(p_1 \cdot p_2))\varepsilon_0^\mu + z(\varepsilon_0 \cdot p_1) p_1^\mu\right] + z(\varepsilon_0 \cdot p_1)(z p_1^2 + y(p_1 \cdot p_2)). \tag{B13}$$

After Wick rotation and the integration over angular variables $\mathrm{d}\Omega_4$, the term proportional to l_μ gives zero and $l_\mu l_\nu \to -g_{\mu\nu}\, l_E^2/4$. So one arrives at

$$\int \frac{\mathrm{d}^4 k_1}{(2\pi)^4\, i} \frac{(\varepsilon_0 \cdot k_1)(k_1 \cdot p_1)}{\Delta_0 \Delta_1 \Delta_2 \Delta_3} = \int_0^1 \mathrm{d}t \int_0^1 \mathrm{d}x \int_0^1 \mathrm{d}y \int_0^1 \mathrm{d}z\, 3!\, \delta(t + x + y + z - 1) \times \\ \times (\varepsilon_0 \cdot p_1) \left[-\frac{1}{4} \int \frac{\mathrm{d}^4 l_E}{(2\pi)^4} \frac{l_E^2}{(l_E^2 + \Delta - i\epsilon)^4} + z(z p_1^2 + y(p_1 \cdot p_2)) \int \frac{\mathrm{d}^4 l_E}{(2\pi)^4} \frac{1}{(l_E^2 + \Delta - i\epsilon)^4}\right]. \tag{B14}$$

All integrals converge. The integration over $\mathrm{d}t$ is removed by a delta-function.

$$\frac{1}{2}\, V_4 = \frac{(\varepsilon_0 \cdot p_1)}{16\pi^2} \left[\int_0^1 \mathrm{d}y \int_0^{1-y} \mathrm{d}z \frac{1}{\Delta_{yz} + m_1^2(1 - y - z) - i\epsilon} + \right. \\ \left. + \int_0^1 \mathrm{d}y \int_0^{1-y} \mathrm{d}z \int_0^{1-y-z} \mathrm{d}x \left(\frac{yz(p_0 \cdot p_1) + z^2 p_1^2}{(\Delta_{yz} + m_1^2 x - i\epsilon)^2} - \frac{1/4}{\Delta_{yz} + m_1^2 x - i\epsilon}\right)\right], \tag{B15}$$

Δ_{yz} is given by equation (B6).

c. Third integral

The calculation of V_5, equation (B3) proceeds similarly to V_4. The difference is that we have four poles instead of three in the denominator of equation (B3). First, one can simplify

the numerator as in equation (B10):

$$\frac{1}{2C}V_5 = (\varepsilon_0 \cdot p_1)\int \frac{\mathrm{d}^4k_1}{(2\pi)^4\, i}\frac{1}{\Delta_1\Delta_2\Delta_3\Delta_4} + \int \frac{\mathrm{d}^4k_1}{(2\pi)^4\, i}\frac{(\varepsilon_0 \cdot k_1)(k_1 \cdot p_1)}{\Delta_0\Delta_1\Delta_2\Delta_3\Delta_4}, \tag{B16}$$

where $\Delta_4 = M^2 - k_1^2$.

We introduce four and five Feynman parameters for the integrals, respectively. The expression for the denominators are D_5^4 and $D_5'^5$:

$$D_5 = x(m_1^2 - k_1^2) + y(m_2^2 - (p_0 - k_1)^2) + z(m_3^2 - (k_1 - p_1)^2) + u(M^2 - k_1^2), \tag{B17}$$

$$D_5' = t(-k_1^2) + x(m_1^2 - k_1^2) + y(m_2^2 - (p_0 - k_1)^2) + z(m_3^2 - (k_1 - p_1)^2) + u(M^2 - k_1^2). \tag{B18}$$

Then we perform the same calculation as in section B 0 b, and the result is

$$\frac{1}{2C}\,V_5 = \frac{(\varepsilon_0 \cdot p_1)}{16\pi^2}\int_0^1 \mathrm{d}y \int_0^{1-y}\mathrm{d}z\int_0^{1-y-z}\mathrm{d}x\left[\frac{1}{(\Delta_{yz} + m_1^2 x + M^2(1-x-y-z) - i\epsilon)^2} + \right.$$
$$\left. + \int_0^{1-x-y-z}\mathrm{d}u\left(\frac{yz(p_0\cdot p_1) + z^2 p_1^2}{(\Delta_{yz} + m_1^2 x + M^2 u - i\epsilon)^3} - \frac{1/4}{(\Delta_{yz} + m_1^2 x + M^2 u - i\epsilon)^2}\right)\right], \tag{B19}$$

where Δ_{yz} is given by equation (B6). To make the expression simpler and convenient for a numerical evaluation, we carry out the integration over $\mathrm{d}x$ and $\mathrm{d}y$ explicitly:

$$\frac{1}{2C}\,V_5 = \frac{1}{16\pi^2}\int_0^1 dy\int_0^{1-y} dz \times$$
$$\left(\frac{(1-y-z)}{(\Delta_{yz} + m_1^2(1-y-z) - i\epsilon)(\Delta_{yz} + M^2(1-y-z) - i\epsilon)} + \right.$$
$$\frac{(z^2 p_1^2 + yz(p_1\cdot p_2))(1-y-z)^2}{(\Delta_{yz} + m_1^2(1-y-z) - i\epsilon)(\Delta_{yz} + M^2(1-y-z) - i\epsilon)(\Delta_{yz} - i\epsilon)} -$$
$$\left. - \frac{1}{4}\frac{2}{M^2}\left[\frac{1}{m_1^2}\log\frac{\Delta_{yz} + m_1^2(1-y-z) - i\epsilon}{\Delta_{yz} - i\epsilon} - \frac{1}{m_1^2 - M^2}\log\frac{\Delta_{yz} + m_1^2(1-y-z) - i\epsilon}{\Delta_{yz} + M^2(1-y-z) - i\epsilon)}\right]\right). \tag{B20}$$

[1] Particle Data Group, K. Olive *et al.*, Chin.Phys. **C38**, 090001 (2014).

[2] E. Klempt and A. Zaitsev, Phys. Rept. **454**, 1 (2007), 0708.4016.

[3] N. Brambilla *et al.*, Eur. Phys. J. C **74**, 2981 (2014), 1404.3723.

[4] COMPASS Collaboration, C. Adolph *et al.*, submitted to Phys. Rev. Lett. (2015), 1501.05732.

[5] COMPASS Collaboration, S. Paul, EPJ Web Conf. **73**, 03002 (2014), 1312.3678.

[6] COMPASS Collaboration, B. Ketzer, PoS **Hadron 2013**, 011 (2014), 1403.4884.

[7] Y. Khokhlov *et al.*, PoS **Hadron2013**, 088 (2014).

[8] J.-J. Wu, X.-H. Liu, Q. Zhao, and B.-S. Zou, Phys.Rev.Lett. **108**, 081803 (2012), 1108.3772.

[9] X.-G. Wu, J.-J. Wu, Q. Zhao, and B.-S. Zou, Phys.Rev. **D87**, 014023 (2013), 1211.2148.

[10] BESIII Collaboration, M. Ablikim *et al.*, Phys.Rev.Lett. **108**, 182001 (2012), 1201.2737.

[11] N. Achasov and A. Kozhevnikov, Z.Phys. **C48**, 121 (1990).

[12] S. Bityukov *et al.*, Phys. Lett. B **188**, 383 (1987).

[13] A. P. Szczepaniak, (2015), 1501.01691.

[14] U. G. Meissner, Phys.Rept. **161**, 213 (1988).

[15] L. Landau, Nucl. Phys. **13**, 181 (1959).

[16] R. Cutkosky, J.Math.Phys. **1**, 429 (1960).

[17] V. N. Gribov, Y. L. Dokshitzer, and J. Nyiri, *Strong Interactions of Hadrons at High Energies – Gribov Lectures on Theoretical Physics* (Cambridge University Press, Cambridge, 2009).

[18] J. M. Blatt and V. F. Weisskopf, *Theoretical Nuclear Physics* (Wiley, New York, 1952).

[19] CLEO Collaboration, D. Asner *et al.*, Phys.Rev. **D61**, 012002 (2000), hep-ex/9902022.

[20] V. Anisovich, A. Kondashov, Y. Prokoshkin, S. Sadovsky, and A. Sarantsev, Phys.Atom.Nucl. **63**, 1410 (2000), hep-ph/9711319.

[21] CLEO Collaboration, R. A. Briere *et al.*, Phys.Rev.Lett. **90**, 181802 (2003), hep-ex/0302028.

[22] CLEO Collaboration, T. Coan *et al.*, Phys.Rev.Lett. **92**, 232001 (2004), hep-ex/0401005.

[23] S. M. Flatte, Phys.Lett. **B63**, 224 (1976).

[24] V. Baru, J. Haidenbauer, C. Hanhart, A. E. Kudryavtsev, and U.-G. Meissner, Eur.Phys.J. **A23**, 523 (2005), nucl-th/0410099.

[25] BES Collaboration, M. Ablikim *et al.*, Phys.Lett. **B607**, 243 (2005), hep-ex/0411001.

[26] R. Garcia-Martin, R. Kaminski, J. Pelaez, and J. Ruiz de Elvira, Phys.Rev.Lett. **107**, 072001

(2011), 1107.1635.

[27] G. Ascoli *et al.*, Phys. Rev. D **9**, 1963 (1974).

[28] VES Collaboration., E. Berdnikov *et al.*, Phys.Lett. **B337**, 219 (1994).